CELLULAR NEUROSCIENCE

Autocrine inhibition by a glutamate-gated chloride channel mediates presynaptic homeostatic depression

Xiling Li[1,2], Chun Chien[1,2], Yifu Han[1,2], Zihan Sun[1], Xun Chen[1,2], Dion Dickman[1]*

Homeostatic modulation of presynaptic neurotransmitter release is a fundamental form of plasticity that stabilizes neural activity, where presynaptic homeostatic depression (PHD) can adaptively diminish synaptic strength. PHD has been proposed to operate through an autocrine mechanism to homeostatically depress release probability in response to excess glutamate release at the *Drosophila* neuromuscular junction. This model implies the existence of a presynaptic glutamate autoreceptor. We systematically screened all neuronal glutamate receptors in the fly genome and identified the glutamate-gated chloride channel (*GluClα*) to be required for the expression of PHD. Pharmacological, genetic, and Ca^{2+} imaging experiments demonstrate that GluClα acts locally at axonal terminals to drive PHD. Unexpectedly, GluClα localizes and traffics with synaptic vesicles to drive presynaptic inhibition through an activity-dependent anionic conductance. Thus, GluClα operates as both a sensor and effector of PHD to adaptively depress neurotransmitter release through an elegant autocrine inhibitory signaling mechanism at presynaptic terminals.

INTRODUCTION

Adaptive plasticity mechanisms act as sentinels at synapses to stabilize neural circuit function, maintaining efficacy while still permitting the flexibility necessary for learning and memory (*1*). These homeostatic signaling systems operate on both sides of the synapse. On the postsynaptic side, much is known about homeostatic receptor scaling, in which the abundance of ionotropic AMPA-type glutamate receptors (GluRs) is adaptively and bidirectionally modulated at synapses (*2*). Homeostatic signaling systems also target the efficacy of presynaptic neurotransmitter release, referred to as presynaptic homeostatic plasticity (*3*, *4*). Homeostatic control of presynaptic function is a fundamental feature of synapses, conserved from invertebrates to humans (*4*). Underscoring their importance, defects in homeostatic signaling have been associated with a variety of neural diseases (*5*). In one well-characterized form of homeostatic plasticity, presynaptic release can be enhanced to compensate for diminished postsynaptic receptor functionality, a process termed presynaptic homeostatic potentiation (PHP). PHP operates to stabilize synaptic strength at neuromuscular junctions (NMJs) of *Drosophila* (*6*, *7*), rodents (*8*), and humans (*9*) and was recently shown to function in the mammalian central nervous system (*10*). While much has been learned about the genes and mechanisms involved in PHP, far less is understood about a seemingly inverse process governing the homeostatic depression of presynaptic neurotransmitter release.

A model for presynaptic homeostatic depression (PHD) has been established at the glutamatergic *Drosophila* NMJ. In this system, neuronal overexpression of the vesicular glutamate transporter *vGlut* (vGlut-OE) enlarges synaptic vesicles, which leads to a concomitant increase in quantal size due to excess glutamate released from individual synaptic vesicles (*7*, *11*). However, evoked synaptic responses are maintained at baseline levels because of a homeostatic decrease in the number of synaptic vesicles released per stimulus (quantal content). PHD is also observed in mutations of genes involved in synaptic vesicle endocytosis, in which enlarged synaptic vesicles are caused by defects in endocytic reformation (*12*–*14*). Subsequent work has demonstrated that PHD requires genes and physiological adaptations that are distinct from the ones known to be involved in PHP (*15*, *16*) and that PHD reduces neurotransmitter release probability by decreasing presynaptic Ca^{2+} influx (*15*) without altering the abundance of endogenous Ca^{2+} channels at active zones (*17*). The only known way to induce PHD is through excess presynaptic glutamate release due to synaptic vesicle enlargement; postsynaptic GluR overexpression enhances quantal size but does not alter presynaptic function (*16*, *18*). The presynaptic neuron appears oblivious to the excitability state of the postsynaptic muscle following PHD adaptation (*16*). Therefore, it was proposed that a "glutamate homeostat" operates at the *Drosophila* NMJ in which enlarged synaptic vesicles and/or excess glutamate release triggers presynaptic inhibition through an autocrine signaling system (*16*). This hypothesis implies the existence of a glutamate autoreceptor that functions to signal PHD. However, the identity of this receptor, if one does exist, is unknown, and not a single gene has yet been identified to be necessary for PHD expression.

Two fundamental pathways have been defined that mediate presynaptic inhibition in diverse nervous systems. First, metabotropic signaling in presynaptic terminals can ultimately lead to diminished neurotransmitter release. For example, metabotropic GluRs located at axonal terminals of mammalian central neurons can modulate presynaptic function, including the inhibition of neurotransmitter release (*19*–*22*). At the fly NMJ, metabotropic GluRs are present at motor neuron terminals where they function to depress the augmentation of evoked responses during high levels of synaptic stimulation (*23*). There is also evidence that presynaptic ionotropic GluRs engage metabotropic pathways and contribute to the potentiation or inhibition of presynaptic release (*24*, *25*). One notable example is illustrated in the rodent hippocampus, where elevated glutamate release inhibits subsequent synaptic release through autocrine activation of presynaptic *N*-methyl-D-aspartate (NMDA)–type GluRs (*26*). A second mechanism for presynaptic inhibition uses a chloride conductance at axonal terminals. In classical studies of the crayfish NMJ, GABAergic axo-axonic synapses onto motor

[1]Department of Neurobiology, University of Southern California, Los Angeles, CA, 90089, USA. [2]USC Neuroscience Graduate Program, Los Angeles, CA, 90089, USA.
*Corresponding author. Email: dickman@usc.edu

neuron terminals drives presynaptic inhibition through a "shunting current" (*27*). Presynaptic inhibition has also been demonstrated at afferent sensory inputs to the spinal cord, where activation of presynaptic GABA (γ-aminobutyric acid) receptors mediates an inhibitory chloride conductance (*28*). Last, the acetylcholine-gated chloride channel LGC-46 drives an activity-dependent autocrine inhibition at the *Caenorhabditis elegans* NMJ (*29*). Notably, both metabotropic and chloride-mediated presynaptic inhibition converge on a reduction in presynaptic Ca^{2+} influx to ultimately diminish neurotransmitter release (*21*, *30*). However, whether and to what extent metabotropic or chloride signaling contributes to PHD at the *Drosophila* NMJ has not been determined.

To elucidate the molecular mechanisms underlying PHD induction and expression, we systematically screened the 11 neural GluRs encoded in the *Drosophila* genome for roles in PHD at the NMJ using an electrophysiological assay. While 10 of the GluRs were dispensable, this approach identified the glutamate-gated chloride channel *GluClα* to be required for PHD expression. Additional studies reveal that GluClα functions locally at motor neuron terminals to drive an activity- and chloride-dependent autocrine inhibition in response to excess glutamate release. GluClα may therefore serve as both sensor and effector to couple enlarged synaptic vesicles and excess glutamate release to an activity-dependent chloride conductance that ultimately serves to homeostatically diminish Ca^{2+} influx at release sites to enable PHD expression.

RESULTS

An electrophysiology-based candidate screen identifies *GluClα* to be required for PHD

To identify the putative glutamate autoreceptor that mediates PHD (Fig. 1A), we systematically screened all 11 GluR genes encoded in the *Drosophila* genome [excluding the known muscle and olfactory GluRs (*31*)]. These 11 GluRs are composed of five evolutionarily distinct families that include homologs of kainate-, AMPA-, and NMDA-type ionotropic GluRs, as well as the single metabotropic (*mGluRA*) and glutamate-gated chloride channels (Fig. 1B). We established a collection of 18 mutants and/or RNA interference (RNAi) lines that disrupt these GluRs from our own studies and/or from public resources to screen for the defects in PHD expression (table S1).

To assess whether PHD can be expressed after disruption of these candidate GluRs, we used an established electrophysiological assay to record synaptic transmission at the larval NMJ. First, we determined baseline transmission by recording miniature and evoked excitatory postsynaptic potentials (mEPSPs and EPSPs); from this data, we estimated the number of synaptic vesicles released per stimulus (quantal content; table S1). To then specifically assess PHD expression, we crossed each mutation or RNAi line into a genetic background in which *vGlut* was overexpressed in motor neurons using the *vGlut* driver *OK371-Gal4* (vGlut-OE) and performed electrophysiological recordings. vGlut-OE induces an increase in mEPSP amplitude, as expected, but EPSP amplitudes are maintained at baseline levels because of a homeostatic decrease in presynaptic glutamate release (quantal content; Fig. 1, C to F). As in controls, vGlut-OE led to a significant increase in mEPSP amplitude in all mutants screened (Fig. 1G and table S1). From the outset, we considered it unlikely that the kainate- and AMPA-type receptors encoded in the fly genome, which generally mediate excitatory currents, would function as autoreceptors to mediate PHD. However, metabotropic functions have been reported for both kainate and AMPA receptors (*24*, *25*, *32*). We found that PHD was robustly expressed in these mutants (Fig. 1G and table S1). Thus, we find no evidence for roles of *Drosophila* kainate- or AMPA-type GluRs in PHD.

Next, we focused on what we considered the most likely candidate GluRs for mediating PHD: NMDA and mGluRA subtypes. In the mammalian hippocampus, presynaptic NMDA receptors can function as autoreceptors to inhibit synaptic vesicle release in response to increased glutamate levels (*26*), and NMDA receptors have also been reported to be present at the fly NMJ (*33*). We found that both *Drosophila* NMDA receptors and the lone metabotropic mGluRA are expressed in the larval central nervous system and motor neurons using GluR expression reporters (fig. S1A). However, unambiguous mutations in the two *Drosophila* NMDA receptors, NMDAR1 and NMDAR2, have not been established. We therefore generated null mutations in both NMDAR1 and NMDAR2 using CRISPR-Cas9 gene editing approaches (see Materials and Methods and table S1). While baseline synaptic function was largely unchanged in these mutants, PHD was robustly expressed following vGlut-OE (Fig. 1G and table S1). We also assessed PHD in mutations of the sole metabotropic GluR encoded in the *Drosophila* genome, *mGluRA*. Metabotropic GluRs can function as autoreceptors to mediate presynaptic inhibition in the mammalian central nervous system (*19*, *22*). Consistent with a conserved function in this process, mGluRA receptors are present at motor neuron terminals at the fly NMJ and function to inhibit neurotransmitter release in response to high levels of synaptic stimulation (*23*). However, null mutations in *mGluRA* show robust PHD expression (Fig. 1, C to F, and table S1). We further tested potential roles for metabotropic pathways in PHD signaling by screening pertussis toxin, which inhibits Gi/o-dependent action, as well as seven additional genes involved in G protein–coupled signaling. However, we found no evidence for functions of any of these pathways in PHD (fig. S1, B and C). Because unambiguous null mutations do not yet exist for a subset the genes screened (namely, the AMPA and a few KARs; table S1), we cannot completely rule out their potential functions in PHD. Nonetheless, through screening of kainate-, AMPA-, NMDA-, mGluRA-, and additional metabotropic signaling factors, we find no evidence for these factors to be involved in PHD at the fly NMJ.

Last, we tested whether the final GluR candidate, *GluClα*, was required for PHD expression. Unexpectedly, PHD failed to be expressed when *vGlut* was overexpressed in a background containing a *GluClα* mutation identified from the MiMIC gene disruption project (*34*). Specifically, although miniature amplitudes were similarly enhanced in *GluClα* + vGlut-OE compared to vGlut-OE alone, no change in quantal content was observed (Figs. 1G and 2, C to G), leading to a nonhomeostatic increase in the evoked amplitude (Fig. 2, C and E). The *GluClα* mutant allele used in the screen results from a MiMIC transposon insertion into an intron in the *GluClα* locus that contains a mutagenic cassette predicted to destabilize the transcript (Fig. 2A), and we named this allele $GluCl\alpha^{1}$. *GluClα* encodes a Cys-loop ligand-gated ion channel, a highly conserved family that includes other *GluCl* homologs in invertebrates and mammalian GABA and glycine receptors (*35*). The crystal structure of a *C. elegans* GluCl has been solved, revealing that these channels are composed of homopentamers (*36*).

We characterized synaptic physiology and PHD expression in *GluClα* mutants in more detail using a two-electrode voltage clamp

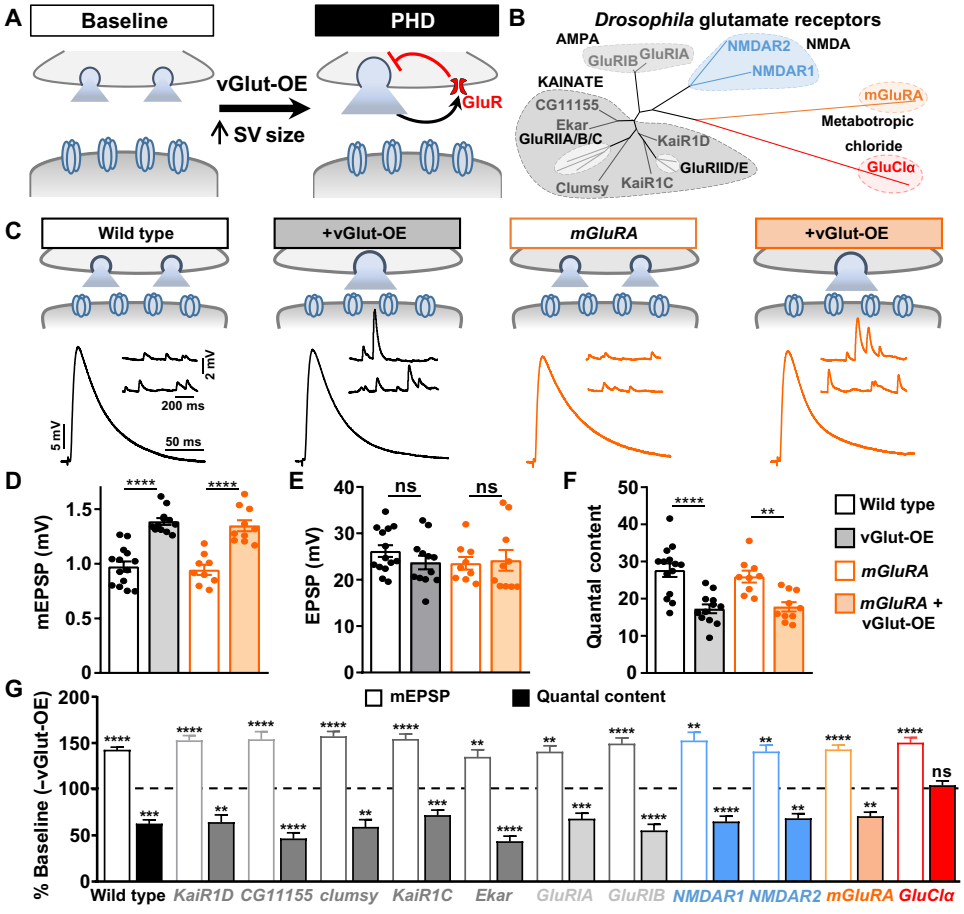

Fig. 1. A screen of *Drosophila* GluRs identifies the glutamate-gated chloride channel to be necessary for PHD. (**A**) Schematic illustrating enlarged synaptic vesicle (SV) size and excess glutamate release following vGlut-OE (*OK371-Gal4/UAS-vGlut*). A putative presynaptic glutamate autoreceptor is shown mediating an autocrine, homeostatic inhibition of neurotransmitter release that drives PHD. (**B**) Phylogenic analysis of putative GluRs encoded in the *D. melanogaster* genome. The maximum likelihood (ML) topology tree is constructed by GluRs separated into the following GluR subtypes: kainate (*10*), AMPA (*2*), NMDA (*2*), metabotropic (*1*), and glutamate-gated (*1*). Note that the five muscle-specific GluR subunits (GluRIIA, IIB, IIC, IID, and IIE) were not screened but are shown in light gray. (**C**) Schematic and representative electrophysiological traces of NMJ recordings from wild-type (w^{1118}) and *mGluRA* mutants ($w;mGluRA^{112b}$) at baseline and following vGlut-OE ($w;UAS\text{-}vGlut/OK371\text{-}Gal4;mGluRA^{112b}$). Increased mEPSP amplitudes are observed in both wild-type and *mGluRA* mutant NMJs after *vGlut* overexpression due to excess glutamate released from individual synaptic vesicles, while EPSP amplitudes are maintained at baseline levels due to a homeostatic decrease in neurotransmitter release (quantal content). (**D** to **F**) Quantification of mEPSP amplitude (D), EPSP amplitude (E), and quantal content (F) in the indicated genotypes (wild type, $n = 14$; +vGlut, $n = 12$; *mGluRA*, $n = 9$; +vGlut, $n = 10$). $^{**}P < 0.01$ and $^{****}P < 0.0001$. (**G**) Quantification of mEPSP amplitude and quantal content in the indicated genotypes normalized to baseline values (–vGlut-OE; $n \geq 8$; see table S1). $^{**}P < 0.01$, $^{***}P < 0.001$, and $^{****}P < 0.0001$. Note that mEPSP amplitudes are enhanced following *vGlut* overexpression in each mutant, while a homeostatic decrease in presynaptic glutamate release (quantal content) is observed in all mutants screened except *GluClα*. The homeostatic inhibition of glutamate release normally induced by vGlut-OE fails to be induced in *GluClα* mutants. ns, not significant.

(TEVC) configuration. No significant differences in baseline synaptic physiology were observed in *GluClα* mutants compared with wild type, including miniature and evoked excitatory postsynaptic current (mEPSC and EPSC) amplitude (Fig. 2, C to F). However, when vGlut-OE was expressed in a *GluClα* mutant background, mEPSC amplitudes were increased as expected, but no homeostatic reduction in quantal content was induced, leading to enhanced EPSC amplitudes (Fig. 2, C to G, and fig. S2, A and B). Similar effects were found when the $GluCl^{1}$ allele was crossed to a deficiency that removed the entire *GluClα* locus (Fig. 2G and table S2), indicating that the $GluCl\alpha^{1}$ allele behaves as a genetic null. We obtained two additional, previously characterized mutant alleles, $GluCl\alpha^{glc}$ and $GluCl\alpha^{FlpStop.D}$ (*37*, *38*), and confirmed that PHD expression is blocked in these alleles as well (Fig. 2, A and G, and table S2), consistent with all three alleles being similar loss-of-function null alleles. Baseline synaptic transmission and PHD expression were not significantly changed in heterozygous conditions of any of these alleles in trans with wild type (table S2). Thus, *GluClα* is required for synapses to express PHD.

We next characterized synaptic structure, function, and plasticity in *GluClα* mutants in more detail. First, we observed no obvious changes in NMJ growth or structure in *GluClα* mutants (fig. S3 and table S2). As previously reported (*16*), the apparent calcium cooperativity of neurotransmission is unaffected in vGlut-OE compared to wild type, and we found no significant difference in calcium cooperativity in $GluCl\alpha^{1}$ + vGlut-OE compared to *GluClα* mutants alone

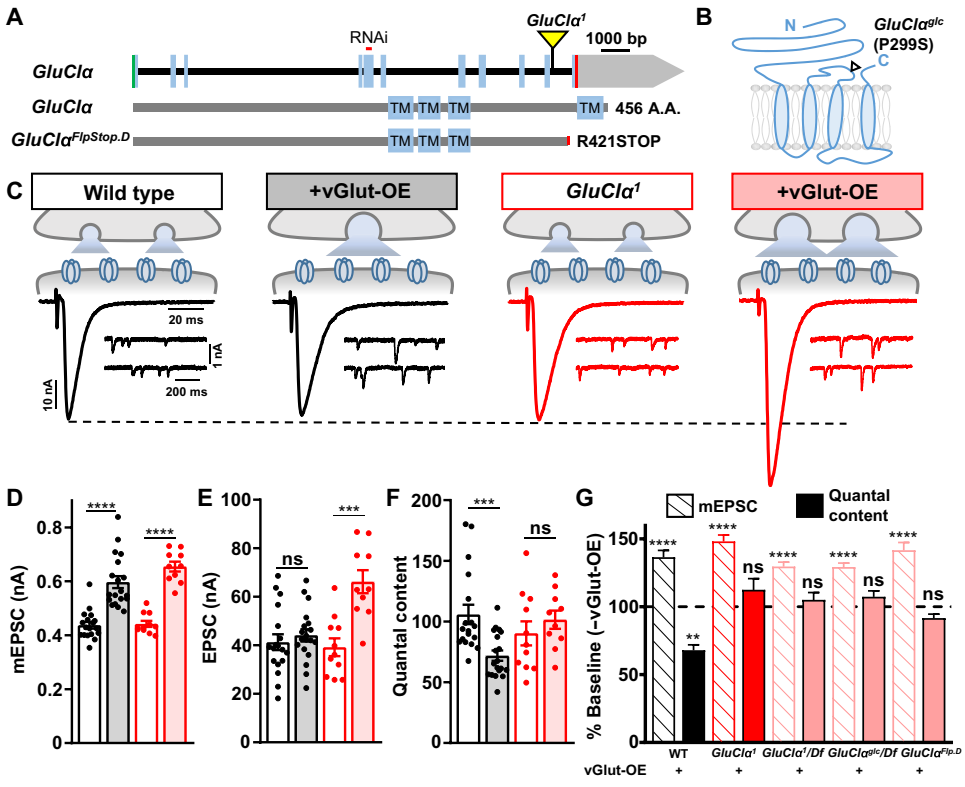

Fig. 2. The glutamate-gated chloride channel *GluClα* is necessary for PHD expression. (**A**) Schematic of the *Drosophila GluClα* locus with the MiMIC transposon insertion causing the *GluClα*^{1} mutation (*GluClα*^{MI02890}) and RNAi targeting sequence shown. Bottom: Protein structure and transmembrane domains of GluClα. (**B**) Diagram of the membrane topology of a single GluClα subunit with the location of the *GluClα*^{glc} mutation illustrated; GluCl channels are homopentamers (*36*). (**C**) Schematic and representative traces of two-electrode voltage clamp NMJ recordings from wild-type (*w*^{1118}) and *GluClα* mutants (*w;GluClα*^{1}) at baseline (*w;OK371-Gal4/UAS-vGlut*) and +vGlut-OE (*w;OK371-Gal4/UAS-vGlut;GluClα*^{1}). Increased mEPSC amplitudes are observed in both wild-type and *GluClα*^{1} NMJs following *vGlut* overexpression. PHD maintains stable evoked amplitude in vGlut-OE NMJs, while EPSC amplitude is significantly enhanced in *GluClα*^{1} + vGlut-OE because of a failure to homeostatically diminish quantal content. (**D** to **F**) Quantification of mEPSC amplitude (D), EPSC amplitude (E), and quantal content (F) values in the indicated genotypes (wild type, $n = 18$; +vGlut-OE, $n = 19$; *GluClα*^{1}, $n = 13$; +vGlut-OE, $n = 10$). ***$P < 0.001$ and ****$P < 0.0001$. (**G**) Quantification of mEPSC and quantal content values normalized to baseline values in the indicated genotypes, including vGlut-OE, *GluClα*^{1} + vGlut-OE and *GluClα*^{1}*/Df* + vGlut-OE (*w;OK371-Gal4/UAS-vGlut;GluCl*^{1}*/Df*), and *GluClα*^{glc}*/Df* + vGlut-OE (*w;OK371-Gal4/UAS-vGlut;GluCl*^{glc}*/Df*). **$P < 0.01$ and ****$P < 0.0001$. bp, base pairs.

(fig. S4, A and B). Furthermore, the probability of neurotransmitter release (P_r), as assessed through failure analysis and short-term plasticity, is reduced in vGlut-OE compared to wild type (fig. S4, C to G) (*11*, *16*). However, no changes in failure rate or short-term plasticity were observed in *GluClα* mutants or *GluClα*^{1} + vGlut-OE compared to wild type (fig. S4C), consistent with a failure to express the adaptations to P_r in *GluClα* mutants that result from PHD. Last, since *GluClα* is required for PHD expression, we considered whether *GluClα* might also be necessary for an inverse homeostatic adaptation well characterized at the *Drosophila* NMJ, PHP. In contrast to PHD, PHP induces increased glutamate release through a homeostatic enhancement in quantal content (*6*). Previous studies have demonstrated that the genes and mechanisms required for PHP do not have roles in PHD (*15*, *16*). Consistent with these findings, we found PHP to be robustly expressed in *GluClα* mutants in response to pharmacological or genetic diminishment of postsynaptic GluRs (fig. S5). Together, these data demonstrate that loss of *GluClα* disrupts PHD expression without significantly affecting baseline synaptic structure or function.

GluClα functions in motor neurons to drive chloride-dependent presynaptic inhibition

In principle, GluClα could function in presynaptic motor neurons and/or the postsynaptic muscle to respond to elevated glutamate released at synapses. Although there is clear evidence that *GluClα* functions in the *Drosophila* central nervous system (*38*, *39*), the peripheral expression of *GluClα* is not known. We cloned a genomic fragment containing the putative *GluClα* promoter upstream of *Gal4* and crossed this to a *GFP* reporter. The *GluClα*-driven green fluorescent protein (GFP) signal is broadly observed in the larval brain and is also expressed in motor neurons that innervate NMJs (Fig. 3A). However, no GFP signal is detected in muscle or peripheral glia (Fig. 3A), suggesting that *GluClα* is exclusively expressed in the nervous system. Consistent with this finding, we observed a similar expression pattern using a recent *GluClα* driver generated by a T2A-Gal4 knock-in strategy (*40*). Next, to assess the presynaptic requirement of *GluClα* in PHD, we opted not to perform a standard rescue experiment because we were concerned that overexpression of *GluClα* alone might induce presynaptic inhibition (see below).

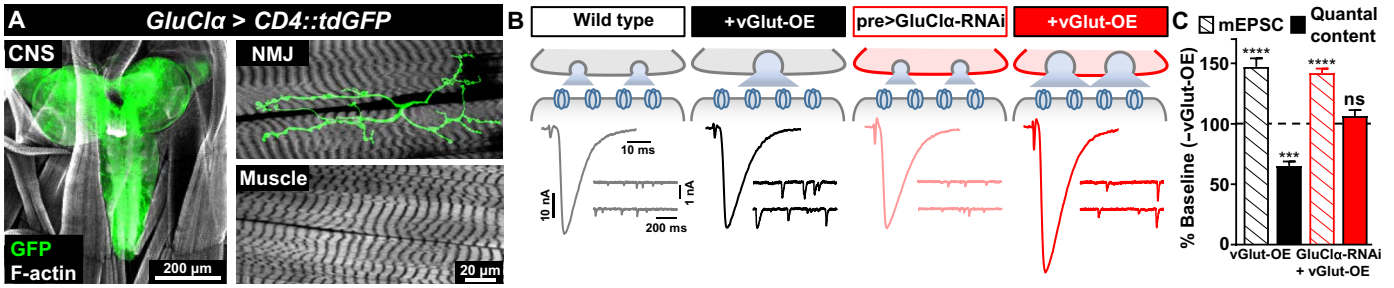

Fig. 3. *GluClα* is expressed in motor neurons and required presynaptically for PHD. (**A**) Representative images of the larval brain [central nervous system (CNS)] and muscle 6/7 NMJ of a GFP reporter driven by the *GluClα* promoter (*w;GluClα-Gal4/UAS-CD4::tdGFP*). Immunostaining using anti-GFP and anti-phalloidin (F-actin marker) is shown. *GluClα* is expressed in the CNS and in motor neurons, while no signal is detected in the muscle. (**B**) Schematic and representative EPSC and mEPSC traces in wild type, vGlut-OE, and following knockdown of *GluClα* expression in motor neurons by RNAi at baseline (pre>GluClα-RNAi: *w;OK371-Gal4/UAS-GluClα RNAi;UAS-Dcr2/+*) and with vGlut-OE (*w;OK371-Gal4/UAS-vGlut,UAS-GluClα RNAi;UAS-Dcr2/+*). PHD fails to be expressed in pre>GluClα-RNAi+vGlut-OE. (**C**) Quantification of mEPSC and quantal content values in the indicated genotypes relative to baseline (wild type, $n = 12$; +vGlut-OE, $n = 13$; pre>GluClα-RNAi, $n = 16$; +vGlut-OE, $n = 20$). ***$P < 0.001$ and ****$P < 0.0001$.

Rather, we used an RNAi transgenic line to knock down *GluClα* specifically in motor neurons. *GluClα* knockdown in motor neurons phenocopied *GluClα* mutants, where baseline neurotransmission was unperturbed and PHD failed to be expressed (Fig. 3, B and C). Thus, *GluClα* is expressed and required in motor neurons to enable PHD.

If GluClα mediates presynaptic inhibition in vGlut-OE through a chloride conductance, then extracellular chloride ions should be necessary for PHD to be expressed at vGlut-OE NMJs. We therefore performed electrophysiological recordings in chloride-free saline, where the anion methanesulphonate was used to substitute for chloride (see Materials and Methods). In chloride-free HL3 (hemolymph-like saline 3) saline, baseline transmission at wild-type NMJs was not significantly different compared to recordings in standard saline, including mEPSC, EPSC, and quantal content values (Fig. 4, A to D). However, in vGlut-OE, mEPSC values were increased, as expected, but EPSC amplitudes were also enhanced because of a failure to homeostatically diminish neurotransmitter release (Fig. 4, A to E). Hence, PHD expression requires extracellular chloride ions to enable presynaptic inhibition.

GluClα functions locally at NMJ terminals to drive presynaptic inhibition

One possibility is that *GluClα* abundance or functionality is enhanced following vGlut-OE to sense and respond to excess glutamate release. We therefore tested whether overexpression of *GluClα* in motor neurons was capable of inducing presynaptic inhibition. We engineered a full length *GluClα* cDNA alone and also with a C-terminal "spaghetti monster" 10xFlag-eGFP epitope [*GluClα::smFP* (*41*)] under the control of Gal4-responsive UAS (Upstream Activating Sequence) sequences. Overexpression of *GluClα* in motor neurons had no impact on mEPSC amplitude (fig. S2C) but led to a ~30% reduction in EPSC amplitude and quantal content (Fig. 5, A to D). A similar depression in evoked release was observed following *GluClα-smFP* overexpression (table S2). Therefore, increased expression of *GluClα* in motor neurons is capable of driving presynaptic inhibition.

We next determined in which subcellular compartment GluClα functions in motor neurons to enable PHD expression. Previous studies have suggested that *GluClα* is located at dendrites and cell bodies of motor neurons, where the application of glutamate can induce inhibitory currents to larval motor neurons (*42*). A recent study demonstrated that GluClα is localized to axonal terminals and dendrites in T4/T5 neurons of the adult *Drosophila* visual system (*39*). Therefore, GluClα could be present at presynaptic terminals of motor neurons to detect and respond to excess glutamate; these distinct locations are schematized in Fig. 6A. To test whether GluClα is functionally present at NMJ terminals, we used the unique pharmacology of GluClα. The insecticide ivermectin (IVM) is a strong agonist of GluClα (*36*), and *Drosophila* GluClα can be irreversibly activated by application of IVM in heterologous cells (*37*). We applied IVM to the semi-intact larval NMJ preparation where, notably, we cut the motor nerve from the cell body before the acute application of IVM and before performing electrophysiological recordings. Application of IVM to a wild-type preparation had no impact on mEPSC amplitude or decay kinetics (table S2), nor was there a significant effect on EPSC rise time (Fig. 6B and table S2). However, a significant reduction in the EPSC decay time constant was observed (Fig. 6, B and C). IVM application did not affect EPSC decay kinetics when applied to *GluClα* mutant NMJs (Fig. 6, B and C). IVM application to vGlut-OE NMJs reduced both the evoked EPSC amplitude and decay time (Fig. 6, B to E), leading to a significant reduction in quantal content (Fig. 6E). Together, these experiments indicate that GluClα channels are functionally present at motor neuron terminals and capable of inhibiting late-releasing synaptic vesicles during single action potentials. Furthermore, these data suggest that following vGlut-OE, there is an apparent increase in the abundance or functionality of GluClα that is likely related to PHD expression.

GluClα colocalizes and traffics with synaptic vesicles at NMJ terminals

Genetic evidence demonstrates that *GluClα* is required in motor neurons to enable PHD, and pharmacological data indicate that GluClα channels are functionally present at motor neuron terminals and capable of mediating local presynaptic inhibition. A recent study has also shown that in central neurons of the Drosophila visual system, GluClα is present not only in dendrites but also at axonal terminals (*39*). If GluClα channels are able to sense excess glutamate released from enlarged synaptic vesicles to induce inhibition,

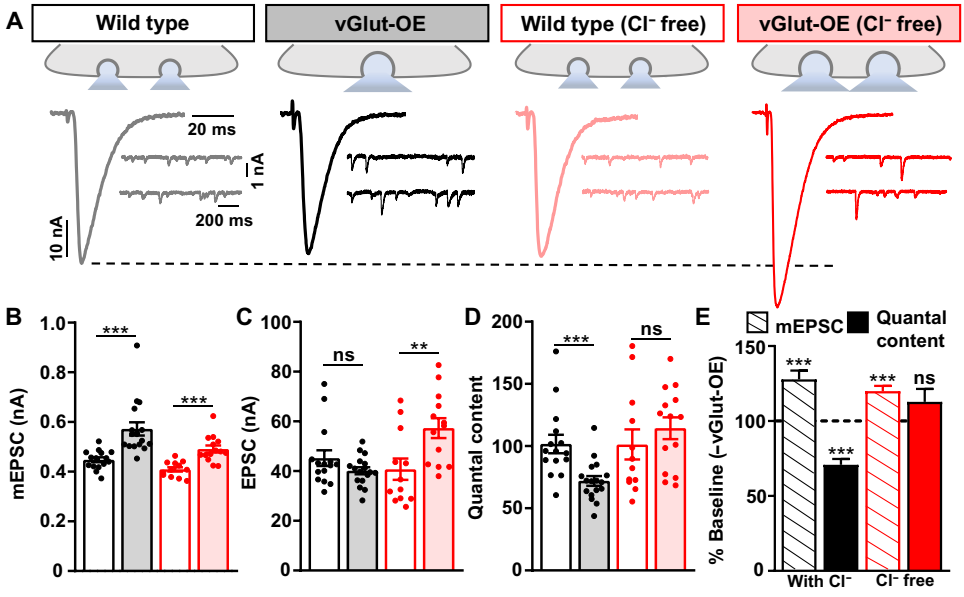

Fig. 4. Extracellular chloride ions are required for PHD expression. (**A**) Schematics and representative traces of mEPSC and EPSC recordings in the indicated genotypes performed in standard or modified (Cl^- free) saline. Although vGlut-OE increases mEPSC amplitude in both saline conditions, no change in presynaptic neurotransmitter release is observed in vGlut-OE NMJs recorded in Cl^--free saline, leading to enhanced EPSC amplitude and a failure to express PHD. (**B** to **D**) Quantification of average mEPSC amplitude (B), EPSC amplitude (C), and quantal content values (D) for the indicated genotypes and conditions (wild type, $n = 15$; vGlut-OE, $n = 17$; wild type Cl^- free, $n = 12$; vGlut-OE Cl^- free, $n = 13$). $^{**}P < 0.01$ and $^{***}P < 0.001$. (**E**) Quantification of mEPSC and quantal content values normalized to baseline values (–vGlut-OE) for wild-type NMJs in standard or Cl^- -free saline. $^{***}P < 0.001$.

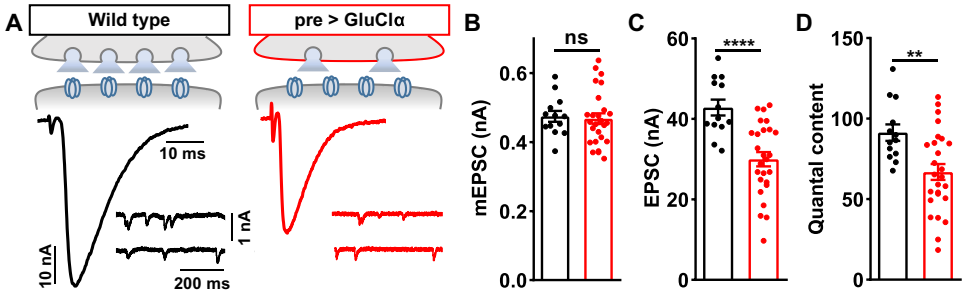

Fig. 5. Presynaptic *GluClα* overexpression diminishes glutamate release. (**A**) Schematic and representative EPSC and mEPSC traces in wild type and presynaptic overexpression of *GluClα* (pre>GluClα: *w;OK371-Gal4/UAS-GluClα*). Presynaptic *GluClα* overexpression reduces EPSC amplitude without significantly changing mEPSCs, indicating diminished neurotransmitter release. (**B** to **D**) Quantification of mEPSC amplitude (B), EPSC amplitude (C), and quantal content (D) in the indicated genotypes (wild type, $n = 10$; pre > GluClα, $n = 13$). $^{**}P < 0.01$ and $^{****}P < 0.0001$.

we hypothesized that these channels should be present at or near release sites where glutamate is secreted. We therefore determined the localization of GluClα by immunostaining *GluClα::smFP* expressed in motor neurons alone and when coexpressed with *vGlut*. Unexpectedly, GluClα::smFP (spaghetti monster fluorescent protein) trafficked to NMJ terminals and colocalized with the synaptic vesicle markers vGlut and synaptotagmin (Syt; Fig. 7A). Furthermore, vGlut signals were increased, while Syt signals were unchanged in vGlut-OE compared to baseline (Fig. 7, A and B), as expected. However, GluClα::smFP signals were also significantly increased when coexpressed with vGlut compared to GluClα::smFP expression alone (Fig. 7, A and B), consistent with increased GluClα incorporating into enlarged synaptic vesicles.

We considered that GluClα::smFP may simply traffic to terminals with synaptic vesicles but that a substantial proportion of GluClα::smFP may be present in the plasma membrane to respond to glutamate. The smFP tag is inserted on the C-terminal tail of GluClα::smFP, which should face the lumen of a synaptic vesicle and the extracellular space if inserted in the plasma membrane (Fig. 7C). To determine the fraction of GluClα::smFP on the plasma membrane, we performed a similar staining as described above but in the absence of the detergent Triton-X-100, thus preventing the anti-Flag antibody from accessing intracellular GluClα::smFP pools (schematized in Fig. 7C). Very little GluClα::smFP signal was found at NMJ terminals in the absence of detergent (Fig. 7, C and D). Thus, GluClα::smFP traffics to NMJ terminals, colocalizes with synaptic vesicle markers, and is predominantly located in intracellular compartments.

Next, we considered that if GluClα channels were indeed incorporated into synaptic vesicles, then these channels should become

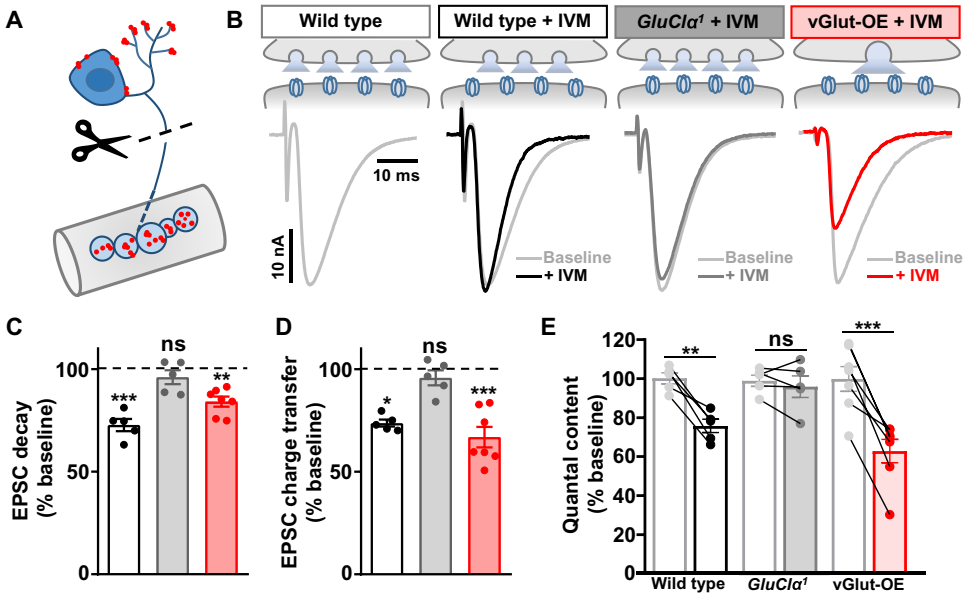

Fig. 6. Acute application of the GluClα agonist IVM induces local presynaptic inhibition. (**A**) Schematic illustrating the putative subcellular locations of GluClα (illustrated in red) at dendrites and axon terminals of motor neurons. Cutting the motor nerve and then applying IVM enables a pharmacological and functional test for the local and acute action of GluClα at motor neuron terminals. (**B**) Schematic and representative EPSC traces in wild type, *GluClα*, and vGlut-OE before (gray) and after (color) IVM application to the same NMJ. IVM application to wild-type NMJs significantly increases the EPSC decay time constant while having no significant effect on *GluClα*-mutant NMJs. In contrast, IVM application to vGlut-OE diminishes EPSC amplitude and decay kinetics, suggesting an increased sensitivity to IVM. (**C**) Quantification of the average EPSC decay time constant of the indicated genotypes after IVM application normalized to baseline (before IVM application) values (wild type, $n = 5$; *GluClα*^{1}, $n = 5$; vGlut-OE, $n = 7$). $^{**}P < 0.01$ and $^{***}P < 0.001$. (**D**) Quantification of the average EPSC total charge transfer in the indicated genotype after IVM application normalized to its baseline value before IVM application (wild type, $n = 5$; *GluClα*^{1}, $n = 5$; vGlut-OE, $n = 7$). $^{*}P < 0.05$ and $^{***}P < 0.001$. (**E**) Quantification of mEPSC and quantal content values in the indicated genotypes after IVM application normalized to baseline values (wild type, $n = 5$; *GluClα*^{1}, $n = 5$; vGlut-OE, $n = 7$). $^{**}P < 0.01$ and $^{***}P < 0.001$.

inserted into the plasma membrane following synaptic vesicle exocytosis. To test this hypothesis, we used a temperature-sensitive allele of *Drosophila dynamin* (*shibire*^{ts1}) to trap synaptic vesicles in the neuronal membrane after fusion. If synaptic vesicles are trapped in the plasma membrane, then the antigens of vGlut and Syt should face the cytosol and no signal should be detected in nonpermeabilized conditions, while the Flag antigen of GluClα::smFP should now face the extracellular space and be labeled (schematized in Fig. 7E). We expressed GluClα::smFP in a *shi* mutant background using larvae in 0 Ca^{2+} saline (rest) at the permissive temperature (22°C) as the control, while synaptic vesicles were fused and trapped in the neuronal plasma membrane by stimulation using high K^{+} saline at the restrictive temperature (34°C). In the absence of Triton, no immunofluorescence signals were detected at rest in the permissive temperature, nor was any vGlut or Syt signal found after high K^{+} stimulation at the restrictive temperature (Fig. 7, E and F), as expected. However, high levels of the GluClα::smFP signal were now found after stimulation at the restrictive temperature (Fig. 7, E and F), strongly suggesting that GluClα::smFP traffics with synaptic vesicles during synaptic stimulation, where it typically remains transiently inserted before being rapidly endocytosed.

Cl^{-} is necessary for the homeostatic reduction in presynaptic Ca^{2+} levels

Last, we hypothesized that PHD is achieved through a homeostatic reduction in presynaptic Ca^{2+} influx driven by Cl^{-}-mediated inhibition. A previous study using Ca^{2+}-sensitive chemical dyes observed a significant reduction in presynaptic Ca^{2+} levels in vGlut-OE (*15*). To determine Ca^{2+} levels at presynaptic boutons, we developed a genetically encoded, ratiometric Ca^{2+} indicator by combining the monomeric, red-shifted Ca^{2+}-insensitive protein mScarlet with the newest and fastest GCaMP variant, GCaMP8f, fused to the synaptic vesicle protein Syt (Fig. 8A; see Materials and Methods). Expression of this transgene in motor neurons revealed the expected colocalization of mScarlet and GCaMP8f with Syt at NMJ boutons (Fig. 8B). We recorded the change in Ca^{2+} induced by single action potential stimulation at individual boutons using high-frequency line scanning (Fig. 8A). We first confirmed the previously observed reduction in Ca^{2+} levels in vGlut-OE compared to wild type (Fig. 8, C and D). However, no change in Ca^{2+} levels was found in vGlut-OE when this experiment was performed in saline lacking Cl^{-} (Fig. 8, E and F). This demonstrates that the reduction in presynaptic Ca^{2+}, which presumably drives the homeostatic modulation of neurotransmitter release necessary for PHD, requires extracellular Cl^{-}. We propose that GluClα mediates an activity-dependent anionic conductance at NMJ terminals, enabling a negative feedback loop that ultimately reduces glutamate release through diminished Ca^{2+} influx at release sites.

DISCUSSION

Through a screen of all 11 neuronal GluRs encoded in the fly genome, we have identified *GluClα* to be necessary for PHD. Our data suggest that GluClα functions locally at nerve terminals to drive homeostatic depression through a chloride-dependent mechanism. GluClα traffics with synaptic vesicles to enable an activity-dependent

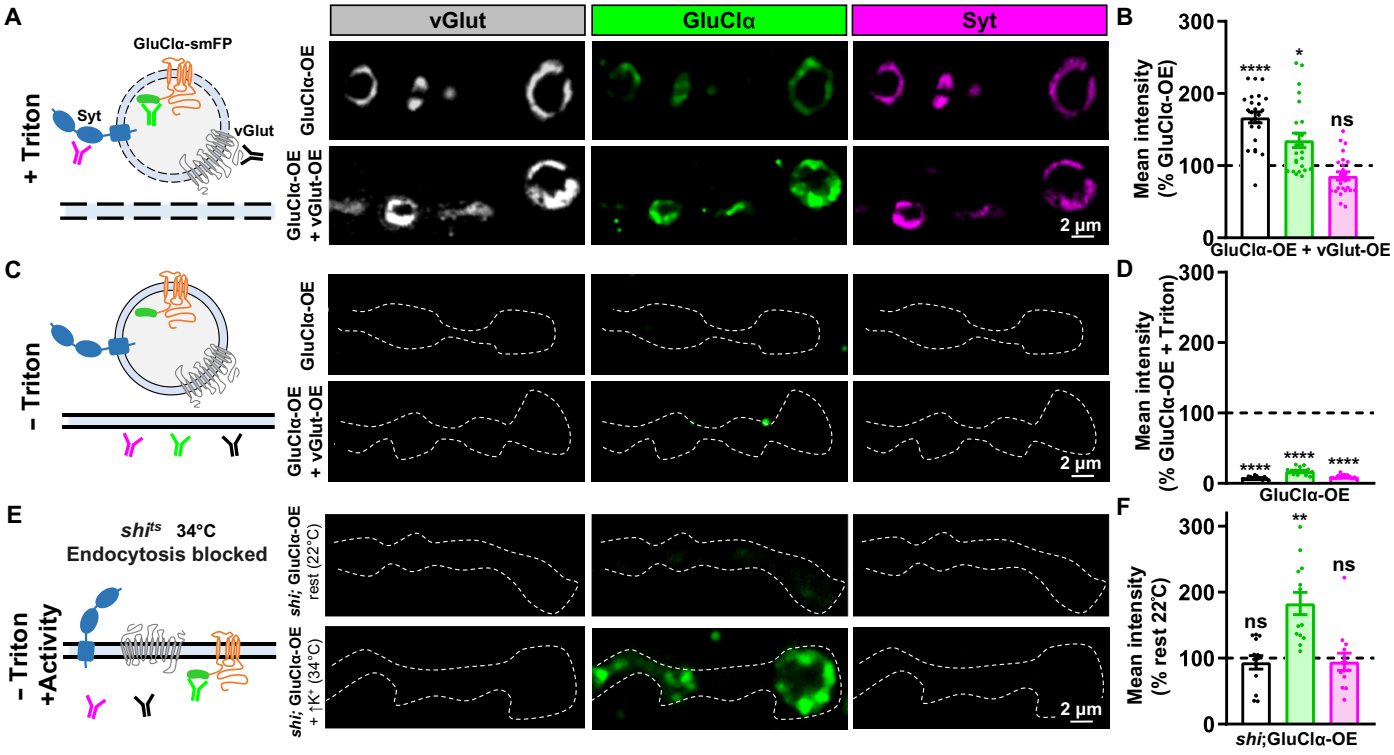

Fig. 7. GluClα colocalizes and traffics with synaptic vesicles. (**A**) Schematic illustrating permeabilized neuronal membrane and antibodies binding to their antigens on synaptic vesicles (left). Representative images of NMJs immunostained for the synaptic vesicle markers vGlut and Syt, as well as GluClα::smFP (anti-Flag) at presynaptic boutons in control (GluClα-OE: *w;OK371-Gal4/UAS-GluClα::smFP*) or in combination with vGlut-OE (GluClα-OE + vGlut-OE: *w;OK371-Gal4/UAS-GluClα::smFP,UAS-vGlut*). (**B**) Quantification of fluorescence intensity of the indicated signals in GluClα-OE + vGlut-OE normalized to GluClα-OE alone. Note that both anti-vGlut and anti-GluClα signals are enhanced, while anti-Syt signals remain unchanged (GluClα-OE, $n = 24$; GluClα-OE + vGlut-OE, $n = 22$). $^{*}P < 0.05$. (**C**) Schematic illustrating nonpermeabilized membrane, in which case the antibodies do not access intracellular compartments. Representative images as described in (A) but in the absence of the detergent Triton. Little antigenic signal was observed in this nonpermeabilized condition, indicating that the majority of GluClα is located in intracellular compartments. The dashed line indicates the neuronal membrane [horseradish peroxidase (HRP) signal]. (**D**) Quantification of fluorescence intensity of nonpermeabilized GluCl-OE staining normalized to the signal found in permeabilized conditions (GluClα-OE, $n = 16$; GluClα-OE + vGlut-OE, $n = 16$). $^{****}P < 0.0001$. (**E**) Schematics of the antigens trapped at the plasma membrane using the temperature-sensitive *shibire* mutant (*shi^{ts}*) at the restrictive temperature (34°C) following high K^+ stimulation. Representative images of NMJs immunostained with synaptic vesicle markers as described in (C) in permissive or restrictive temperatures without membrane permeabilization. (**F**) Quantification of fluorescence intensities of the indicated antigens in *shi^{ts1};OK371-Gal4/UAS-GluCl-smFP* at 34°C after high K^+ normalized to the baseline signal at 22°C. $^{**}P < 0.05$.

anionic conductance at presynaptic terminals that is necessary to reduce presynaptic Ca^{2+} levels. Thus, GluClα acts as an autoreceptor to couple increased vesicular glutamate release with inhibition to adaptively recalibrate neurotransmitter release probability.

GluClα as the sensor and effector of PHD

The induction of PHD, as articulated at the fly NMJ, is intimately associated with enhanced synaptic vesicle size. PHD is observed following overexpression of *vGlut* (*11*, *15*, *16*) and in synaptic vesicle endocytosis mutants where vesicle size is increased because of defective vesicle reformation (*12*–*14*). Therefore, the finding that GluClα traffics with synaptic vesicles suggests that the abundance of this channel may scale with vGlut levels and/or vesicle size. Such a relationship would enable an elegant coupling of GluClα with vesicle size and may actually suggest the possibility that GluClα functions not as a sensor of excess glutamate itself but rather a sensor of synaptic vesicle size. By extension, PHD itself may be a form of adaptive plasticity designed to respond to increased synaptic vesicle size. Since a single vGlut transporter is sufficient to fill a vesicle (*43*), vesicle size should largely determine glutamate content. By scaling inhibition with vesicle size through GluClα, this relationship would tune inhibition to glutamate content. Similar to GluClα, several other factors associated with synaptic vesicles also couple synaptic vesicle fusion with adaptive responses at synapses, including Syt and endophilin, which traffic on or with synaptic vesicles to couple exocytosis with endocytic rates during activity (*44*, *45*), as well as the Ca^{2+} channel Flower, which traffics with synaptic vesicles to drive Ca^{2+} influx after exocytosis to accelerate endocytosis (*46*). GluClα receptors also traffic to axonal terminals in the adult fly visual system (*39*), suggesting the potential for parallel autocrine functions in presynaptic inhibition in the brain. This novel presynaptic function for GluClα, in addition to established actions in driving inhibition at dendrites, may subserve a uniquely specialized role to couple vesicle size with adaptive inhibition.

In contrast to coupling synaptic vesicle size to PHD, there appears to be a distinct and conserved mechanism to drive adaptive presynaptic inhibition in response to enhanced synaptic activity. Here, increased synaptic stimulation leads to increased global glutamate release without changing synaptic vesicle size. In response, presynaptic GluRs initiate metabotropic signaling to adaptively inhibit

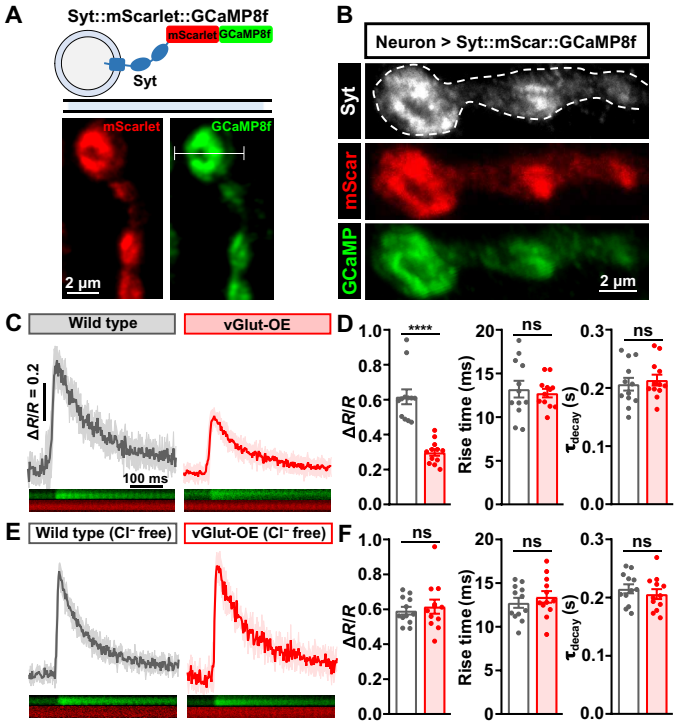

Fig. 8. PHD is achieved through a Cl^--dependent reduction in presynaptic Ca^{2+}. (**A**) Schematic and live confocal images of the Syt::mScarlet::GCaMP8f ratiometric Ca^{2+} reporter. The white line indicates a line scan across a single bouton. (**B**) Representative images of NMJ boutons stained with anti-Syt and endogenous signals of mScarlet and GCaMP8f. (**C**) Representative averaged trace of single action potential–evoked Ca^{2+} transients ($\Delta R = F_{488}/F_{561}$) across time normalized to the baseline F_{488}/F_{561} ratio (R) before stimulation in the indicated genotypes: wild type (*w;OK371-GAL4/+;UAS-syt-mScarlet-GCaMP8f/+*) and vGlut-OE (*w;OK371-GAL4/UAS-vGlut;UAS-syt-mScarlet-GCaMP8f/+*). SEM of 10 independent single action potential–evoked traces is shown in the shaded area (wild type, $n = 12$; vGlut-OE, $n = 12$). (**D**) Quantification of $\Delta R/R$, rise time (10 to 90% to peak), and decay time constant (τ_{decay}) at individual boutons in the indicated genotypes in (C). ****$P < 0.0001$. (**E**) Representative averaged trace of the same experiment and genotypes shown in (C) in 0 Cl^- HL3 saline (wild type, $n = 12$; vGlut-OE, $n = 12$). (**F**) Quantification as described in (D) but of the data shown in (E).

release. This phenomenon has been described at the *Drosophila* NMJ by *mGluRA* (*23*) and in the rodent brain by mGluRs and NMDA receptors (*19*, *20*, *26*). A similar adaptive reduction in release that does not alter synaptic vesicle size may also be induced in cases of synaptic overgrowth at the fly NMJ to maintain stable synaptic strength (*47*, *48*). Note that enhanced glutamate release is also induced by postsynaptic receptor perturbation, the process referred to as PHP. It would seem possible that GluClα could serve to inhibit excess glutamate release in the context of this form of adaptive plasticity. However, we find no evidence that *GluClα* is involved in PHP (fig. S5), consistent with GluClα and PHD being uniquely dedicated to perturbations involving increased synaptic vesicle size. Although glutamate-gated chloride channels are not conserved in mammals, *vGlut* overexpression in rodents does increase quantal size (*49*) similarly to that observed in *Drosophila*. There is a chloride conductance present in mammalian synaptic vesicles that is necessary to properly fill vesicles with glutamate (*50*). Although further studies will be needed to understand how vesicle size, glutamate transport through vGlut, and chloride conductance are regulated in synaptic vesicles, it is possible that GluClα in flies serves a core function subsumed by other processes in mammals. Thus, the GluClα-dependent mechanism for adaptive presynaptic inhibition may be one of a number of strategies synapses have developed to compensate for excess glutamate release.

How might GluClα abundance and/or activity ultimately modulate synaptic function during PHD signaling? Previous Ca^{2+} imaging experiments suggested that the homeostatic reduction in presynaptic glutamate release is achieved through diminished Ca^{2+} levels at presynaptic terminals following synaptic stimulation (*15*), which we confirmed using a new ratiometric, genetically encoded GCaMP8f reporter (Fig. 8). However, there is no apparent change in the abundance of endogenously tagged Ca^{2+} channels at active zones as a result of PHD adaptation (*14*, *17*). Together, these observations suggest that Ca^{2+} levels are functionally modulated during PHD adaptation. The majority of Ca^{2+} influx through P/Q voltage-gated Ca^{2+} channels happens during the "tail current" of the repolarization phase of the action potential (*51*, *52*). Therefore, autocrine inhibitory currents through GluClα channels may accelerate this repolarization and reduce Ca^{2+} influx at active zones, homeostatically tuning synaptic vesicle release. Glutamate autoreceptors can modulate release during single action potentials (*25*, *53*). This model is also consistent with no change exhibited in the readily releasable vesicle pool in PHD (*16*). Additional lines of evidence support the possibility that the abundance of GluClα channels scale with synaptic vesicle size. Baseline transmission is mildly sensitive to the GluClα agonist IVM, where EPSC decay is accelerated (Fig. 6), while EPSC amplitude itself is inhibited by GluClα-OE (Fig. 5) and vGlut-OE after IVM application (Fig. 6). This effect on reducing EPSC amplitude likely reflects an increased GluClα-dependent inhibitory current that alters Ca^{2+} dynamics at earlier stages of the action potential compared to baseline conditions, in which late-releasing vesicles are differentially affected. Furthermore, increased levels of GluClα::smFP are observed in vGlut-OE (Fig. 7). Although GluClα channel abundance scaling with synaptic vesicle size provides an elegant mechanism to tune autocrine inhibition with vesicle size, it is possible that GluClα could traffic through a separate, activity-dependent membrane trafficking pathway to the plasma membrane, a process for which there is precedence (*54*). Such a pathway would need to be extremely rapid for GluClα-mediated inhibitory currents to diminish release of synaptic vesicles during a single action potential. It is difficult to picture such a mechanism working without GluClα actually trafficking with synaptic vesicles, and hence, we consider such a model unlikely. Conversely, it would be interesting to test whether smaller synaptic vesicles contain less GluClα and accordingly impose less inhibition, although it is not clear at present what mutations or manipulations would enable a diminishment of synaptic vesicle volume to test this possibility. GluClα-mediated inhibition provides an analog control mechanism to enable the homeostatic tuning of Ca^{2+} influx and neurotransmitter release probability with synaptic vesicle size.

Synaptic control of glutamate homeostasis

PHD has been presumed to function as a synaptic homeostat designed to maintain proper levels of synaptic strength, similar to PHP but inverse in direction (*11*, *15*). In contrast, PHD was recently proposed to function as a glutamate homeostat, operating as a sentinel against glutamate imbalance (*16*). Homeostatic control of

glutamate levels in the nervous system is crucial. Excess ambient glutamate leads to excitotoxicity, seizures, stroke, and neurodegeneration. vGlut-OE itself drives neurodegeneration in the *Drosophila* brain (*55*). To avoid this toxicity, nervous systems have evolved numerous clearance mechanisms to control and sequester glutamate, with the major mechanism being glutamate transporters located in glia and neurons (*56*). Although the fly genome encodes a single glutamate transporter, *dEAAT1*, that functions in glutamate clearance in the brain and adult periphery, this transporter is not expressed in the larval peripheral nervous system (*57*). Therefore, PHD may actually be a primary mechanism that maintains glutamate balance in the larval periphery.

Adaptive plasticity at synapses controlling presynaptic glutamate release may provide a complementary mechanism with transporter-based clearance to achieve and maintain glutamate homeostasis. A variety of negative feedback mechanisms exist at synapses in other systems that use autocrine inhibition. In addition to the processes discussed above that use GluRs to drive inhibition, it is possible that parallel chloride-based autocrine inhibition mechanisms exist. *GluClα* is a close homolog to mammalian glycine receptors. There is evidence for glutamate and glycine co-release in the mouse visual system (*58*), and presynaptic glycine receptors can influence glutamate release (*59*). In addition, GABA receptors are present at presynaptic terminals (*60*), and a recent study demonstrated that glutamate and GABA can also be co-released (*61*). Such co-release of glutamate and glycine or GABA may enable an autocrine inhibitory current at glutamatergic synapses analogous to PHD at the *Drosophila* NMJ. Thus, autocrine inhibition of glutamate release may be a fundamental mechanism that ensures glutamate balance in the nervous system.

MATERIALS AND METHODS

Experimental model and subject details

Drosophila stocks were raised at 25°C on standard molasses food in an incubator with a 12-hour light/12-hour dark cycle. All experimental flies were collected at the wandering third-instar larval stage. No significant sex differences were observed in this study. An isozygous w^{1118} strain was used as the wild-type control unless otherwise noted because this is the genetic background in which all genotypes are bred. Each genotype used in this study, including transgenic lines, were backcrossed into this same genetic background for at least five generations. A complete list of all *Drosophila* stock sources and genotypes used in this study can be found in tables S1 and S2. All Institutional Review Board guidelines were followed.

Fly stocks

Drosophila stocks were raised at 25°C on standard molasses food. The w^{1118} strain is used as the wild-type control unless otherwise noted, as this is the genetic background of the transgenic lines and other genotypes used in this study. The fly stocks used in this study are detailed in the table S3. The complete list of all GluR alleles screened is detailed in table S1.

Molecular biology

There are 11 predicted *Drosophila GluClα* isoforms based on expressed sequence tags (http://flybase.org/reports/FBgn0024963.html). Among the isoforms, *GluCl-RM* appears to be the major one based on reverse transcription polymerase chain reaction (PCR) from *Drosophila* heads (*37*). To generate *UAS-GluClα*, we cloned the full-length *GluClα-RM* cDNA by reverse transcription of total RNA samples extracted from adult heads of the w^{1118} strain and inserted this sequence into the pACU2 vector (31223, Addgene, Cambridge, MA). Separately, a spaghetti monster *10xFLAG GFP* tag (*41*) was PCR-amplified and placed in-frame before the stop codon of the *GluClα* open reading frame to generate *pACU2-GluClα::smFP*. The Gibson Assembly Cloning Kit (New England Biolabs Inc., E5510S) was used to generate the final construct. To generate UAS-Syt::mScarlet::GCaMP8f, we obtained the previously engineered UAS-Syt::GCaMP6s plasmid (*62*) and replaced the GCaMP6s sequence with sequences encoding mScarlet (85069, Addgene) and GCaMP8f (162379, Addgene). This construct was injected into the VK27 insertion site by BestGene Inc. (Chino Hill, CA). To generate the *GluClα* promotor fusion with *Gal4*, a PCR fragment of 3.98 kb upstream of the *GluClα* transcriptional start site was cloned into the pDEST-APIGH vector to drive *Gal4* expression. This construct was injected into the VK18 insertion site by BestGene Inc.

We generated NMDAR1 and NMDAR2 mutants using a CRISPR-Cas9 genome editing strategy (*63*, *64*). Briefly, we selected three target Cas9 cleavage sites in the first coding exon of NMDAR1 [single guide RNAs (sgRNAs): CCCTCGACGTACAACATTGG; TCCGCATGGACAAGAATCCC; GGTGCCGCCGTACTACCACC] and NMDAR2 (sgRNA: ATGATGAACAACGAACAGTT; AACCGGGATGCCCAGGTAGC; GGAGGCCTACCTAACGGATC) without obvious off-target sequences in the *Drosophila* genome. DNA sequences covering these target sequences were synthesized and subcloned into the pAC-U63-tgRNA-Rev vector (*65*). This plasmid was then injected into the attP40 insertion site by BestGene Inc. These sgRNA stocks were crossed to *vas-Cas-9* (*63*), and 20 putative mutant lines were generated, with the relevant locus amplified by PCR and sequenced. Independent deletions or insertions with predicted frameshifts leading to early stop codons were isolated, which indicated null mutations in the *NMDAR1* open reading frame, named $NMDAR1^{XC1}$ (R80H…L104STOP) and $NMDAR1^{XC3}$ (I41W…L54STOP). Two similar alleles were obtained in *NMDAR2*, named $NMDAR2^{YH7}$ (G14A…C40STOP) and $NMDAR2^{YH9}$ (L71F…A178STOP).

Immunocytochemistry

Larvae were dissected in ice-cold 0 Ca^{2+}-modified HL3 saline (*12*) containing 70 mM NaCl, 5 mM KCl, 10 mM $MgCl_2$, 10 mM $NaHCO_3$, 115 mM sucrose, 5 mM trehelose, and 5 mM Hepes (pH 7.2) and immunostained as described (*64*). Briefly, dissected larvae were washed three times with modified HL3 saline and fixed in Bouin's fixative (HT10132-1L, Sigma Chemical, St. Louis, MO) for 5 min. Larvae were washed with phosphate-buffered saline containing 0.1% Triton X-100 (PBST) and blocked with 5% normal donkey serum followed by incubation in primary antibodies at 4°C overnight. The following day, larvae underwent three 10-min washes in PBST (or PBS to prevent membrane permeabilization) and were incubated in secondary antibodies at room temperature for 2 hours. Samples were transferred in VECTASHIELD (Vector Laboratories, Burlingame, CA) and mounted on glass cover slides. The following antibodies were used: guinea pig anti-vGlut (1:2000) (*66*), rabbit anti-SYT1 (1:2500) (*67*), and mouse anti-flag (1:1000; Sigma-Aldrich, F1804). Donkey anti-mouse, anti-guinea pig, and anti-rabbit Alexa Fluor 488–conjugated (715-545-150, 706-545-148, and 711-545-152; Jackson ImmunoResearch); DyLight 405–conjugated (715-475-150, 706-475-148, and 711-475-152; Jackson ImmunoResearch); and cyanine 3–conjugated (715-165-150, 706-165-148, and 711-165-152; Jackson ImmunoResearch) secondary antibodies were used at 1:400.

Tetramethylrhodamine-conjugated phalloidin (R415, Thermo Fisher Scientific) and Alexa Fluor 647–conjugated goat anti–horseradish peroxidase (HRP) (123-605-021, Jackson ImmunoResearch) were used at 1:200.

Confocal imaging and analysis

Samples were imaged using a Nikon A1R resonant scanning confocal microscope equipped with NIS-Elements software and a 100× APO (Apochromatic) 1.4 numerical aperture (NA) or 20× 1.4 NA oil immersion objective using separate channels with four laser lines (405, 488, 561, and 637 nm) at room temperature. Both type Ib and Is boutons on muscle 6/7 of segments A2 and A3 were counted by considering vGlut and HRP-stained NMJ terminals. For fluorescence quantifications of synaptic vesicle markers and GluClα::smFP, all genotypes within a dataset were immunostained in the same tube with identical reagents and then mounted and imaged in the same session. *z* stacks were obtained using identical settings for all genotypes, with *z*-axis spacing between 0.15 and 0.25 μm within an experiment and optimized for detection without saturation of the signal. Maximum intensity projections were used for quantitative image analysis with the NIS-Elements Software General Analysis toolkit. All quantifications were performed for type Ib boutons on muscle 6/7 and muscle 4 of segments A2 and A3. Measurements were taken from at least 10 synapses acquired from at least six different animals. For all images, fluorescence intensities were quantified by applying intensity thresholds to the relevant channel, and the mean puncta intensity was calculated as the total fluorescence intensity signal of the puncta divided by the area of the puncta.

The experiments using *shibire* to trap synaptic vesicles on the plasma membrane after exocytosis were performed as previously described (*12*). Briefly, *shi^{ts1};OK371-Gal4/UAS-GluClα::smFP* larvae were dissected in ice-cold HL3 and then transferred to 0 Ca^{2+}-HL3 saline at 34°C for 2 min to acclimate. Preparations were then incubated in high K^+ saline [15 mM NaCl, 115 mM sucrose, 60 mM KCl, 10 mM $MgCl_2$, 1.5 mM $CaCl_2$, 10 mM $NaHCO_3$, 5 mM trehalose, and 5 mM Hepes (pH 7.2)] at 34°C for 10 min. After stimulation, the samples were transferred to Ca^{2+}-free saline (34°C) briefly and then fixed in Bouins and washed with PBS to prevent membrane permeabilization. The samples were labeled with anti-vGlut, anti-Flag, anti-Syt, and HRP primary antibodies and imaged and quantified as described above.

Ca^{2+} imaging

Third-instar larvae were dissected in modified HL3 saline. Dissected larvae were imaged using a Nikon A1R confocal microscope equipped with NIS-Elements software and a 60× APO 1.0 NA water immersion objective as described (*68*). Imaging was performed in either modified standard HL3 saline or 0 Cl^- saline containing 1 mM Ca^{2+}. Single stimuli were evoked using a Master-9 Pulse Stimulator and an ISO-Flex Stimulus Isolator (A.M.P.I.) at 1 Hz and 0.5-ms duration. Line scans across single boutons were acquired at 521 Hz with 488- and 561-nm lasers during 120-s imaging sessions from multiple boutons in at least two different larvae. Mean fluorescence ratios (R) were calculated as F_{488}/F_{561} of each line scan at a region of interest (ROI). Fluorescence amplitudes for each evoked event was quantified as $\Delta R/R = (R(t) - R_{baseline})/R_{baseline}$, where $R(t)$ is the fluorescence ratio in an ROI at any time point and $R_{baseline}$ is the mean fluorescence ratio of the 2-s period obtained before the onset of the evoked event. The Ca^{2+} transient for each ROI is averaged for 10 single stimulation events. Imaging data with severe muscle movements or fluorescence decay in the 561 channel were rejected. The time constant (τ) of the decay phase for each Ca^{2+} transient was calculated using a monoexponential fit to the transient decay when extrapolated backward to the time of peak fluorescence. Data analysis was performed using custom Jupyter Note codes.

Electrophysiology

All dissections and recordings were performed in modified HL3 saline (*12*, *53*) at room temperature containing the following: 70 mM NaCl, 5 mM KCl, 10 mM $MgCl_2$, 10 mM $NaHCO_3$, 115 mM sucrose, 5 mM trehalose, 5 mM Hepes, and 0.4 mM $CaCl_2$ (unless otherwise specified; pH 7.2) as described (*69*). Recordings were performed on an Olympus BX61WI microscope using a 40×/0.80 NA water-dipping objective and acquired using an Axoclamp 900A amplifier, Digidata 1440A acquisition system, and pCLAMP 10.5 software (Molecular Devices). Electrophysiological sweeps were digitized at 10 kHz and filtered at 1 kHz. For the PHD screen, sharp electrode (electrode resistance between 10 and 25 megohms) recordings were performed on muscles 6 or 7 of abdominal segments A2 or A3 in wandering third-instar larvae. Muscle input resistance (R_{in}) and resting membrane potential (V_{rest}) were monitored during each experiment. Recordings were rejected if the V_{rest} was more depolarized than −60 mV or if the R_{in} was less than 5 megohms. TEVC recordings were performed on muscle 6 of abdominal segments A2 and A3 as described (*68*, *69*). In all TEVC recordings, muscles were clamped at −70 mV with a leak current of absolute value below 5 nA.

mEPSPs or mEPSCs were recorded for 1 min from each muscle cell in the absence of stimulation. Twenty evoked responses (EPSPs or EPSCs) were acquired for each cell under stimulation at 0.5 Hz using 0.5-ms stimulus duration and with stimulus intensity adjusted with an ISO-Flex Stimulus Isolator (A.M.P.I.). Averaged mEPSPs (or mEPSCs) and EPSPs (or EPSCs) were calculated for each recording, and quantal content (QC) was determined for each genotype by the equation: QC = EPSC/mEPSC or EPSP/mEPSP. Failure analysis was performed in 0.18 mM Ca^{2+} modified HL3. The number of failures was quantified during 50 evoked responses using the same stimulation protocol for EPSP/EPSC recordings. To acutely block postsynaptic receptors, larvae were incubated with or without philanthotoxin-433 (PhTx; 20 μM, Sigma-Aldrich) in modified HL3 for 10 min before recordings. Data were analyzed using Clampfit (Molecular Devices), MiniAnalysis (Synaptosoft), and Excel (Microsoft) software.

For acute pharmacological activation of GluClα, EPSCs were recorded with 50 continuous stimuli delivered to the cut motor axons at 0.5 Hz. During this protocol, the bath saline was perfused with 0.4 mM Ca^{2+}-modified HL3 containing 10 μM IVM (Millipore Sigma, I8898) after the 20th stimulation. Average EPSC amplitude for each genotype before the drug was calculated from the 1st to 20th stimuli, and the average EPSC amplitude after IVM treatment was assessed from the 30th to 50th stimuli. The recordings acquired in the chloride-free saline were done as described above. Chloride-free saline was composed of modified HL3 in which the NaCl, KCl, $MgCl_2$, and $CaCl_2$ chemicals were replaced with methylsulfate sodium salt (Sigma-Aldrich, 318183), potassium methaesulfonate (Sigma-Aldrich, 83000), magnesium nitrate hexahydrate (Sigma-Aldrich, 63084), and calcium nitrate tetrahydrate (Sigma-Aldrich, C1396) with the same final ionic concentrations.

Phylogenetic GluR sequence analysis

Phylogenetic analysis was conducted using amino acid sequence alignments for the 11 GluR sequences culled from the

Drosophila melanogaster genome in MEGAX. If more than one isoform was present, the shortest isoforms with essential functional domains were chosen for the analysis to avoid discrepancy arising from different isoforms. The maximum likelihood (ML) fits of 56 different amino acid substitution models were tested, with the best model estimated by MEGAX, and GluR amino acid sequence relationships were obtained using the ML tree reconstruction method and Le-Gascuel model. Initial tree(s) for the heuristic search were obtained by applying the neighbor-joining method to a matrix of pairwise distances estimated using a JTT (Jones-Taylor-Thornton) model. A discrete gamma distribution was used to model evolutionary rate differences among sites [five categories (+G, parameter = 2.0465)]. The tree is drawn to scale, with branch lengths measured in the number of substitutions per site.

Statistical analysis

Data were compared using either a one-way analysis of variance (ANOVA) followed by Tukey's multiple comparisons test or a Student's *t* test (where specified). For analysis of miniature distribution, a Kolmogorov-Smirnov test was used to assess the significance between indicated genotypes. *P* values were obtained: ns (not significant), $*P < 0.05$ (significant), $**P < 0.01$, $***P < 0.001$, and $****P < 0.0001$. Asterisks indicate statistical significance using one-way ANOVA followed by multiple comparisons. Data were analyzed using GraphPad Prism or Microsoft Excel software. Error bars indicate ±SEM. *n* values indicate biologically independent cells. Additional statistical information and absolute values for normalized data in relevant figures can be found in tables S1 and S2.

SUPPLEMENTARY MATERIALS

Supplementary material for this article is available at https://science.org/doi/10.1126/sciadv.abj1215

View/request a protocol for this paper from *Bio-protocol*.

REFERENCES AND NOTES

1. G. Turrigiano, Homeostatic synaptic plasticity: Local and global mechanisms for stabilizing neuronal function. *Cold Spring Harb. Perspect. Biol.* **4**, a005736 (2012).
2. K. Pozo, Y. Goda, Unraveling mechanisms of homeostatic synaptic plasticity. *Neuron* **66**, 337–351 (2010).
3. I. Delvendahl, M. Muller, Homeostatic plasticity-a presynaptic perspective. *Curr. Opin. Neurobiol.* **54**, 155–162 (2019).
4. G. W. Davis, M. Muller, Homeostatic control of presynaptic neurotransmitter release. *Annu. Rev. Physiol.* **77**, 251–270 (2015).
5. J. Wondolowski, D. Dickman, Emerging links between homeostatic synaptic plasticity and neurological disease. *Front. Cell. Neurosci.* **7**, 223 (2013).
6. C. A. Frank, T. D. James, M. Muller, Homeostatic control of Drosophila neuromuscular junction function. *Synapse* **74**, e22133 (2020).
7. P. Goel, D. Dickman, Synaptic homeostats: Latent plasticity revealed at the Drosophila neuromuscular junction. *Cell. Mol. Life Sci.* **78**, 3159–3179 (2021).
8. X. Wang, J. M. McIntosh, M. M. Rich, Muscle nicotinic acetylcholine receptors may mediate trans-synaptic signaling at the mouse neuromuscular junction. *J. Neurosci.* **38**, 1725–1736 (2018).
9. S. G. Cull-Candy, R. Miledi, A. Trautmann, O. D. Uchitel, On the release of transmitter at normal, myasthenia gravis and myasthenic syndrome affected human end-plates. *J. Physiol.* **299**, 621–638 (1980).
10. I. Delvendahl, K. Kita, M. Muller, Rapid and sustained homeostatic control of presynaptic exocytosis at a central synapse. *Proc. Natl. Acad. Sci. U.S.A.* **116**, 23783–23789 (2019).
11. R. W. Daniels, C. A. Collins, M. V. Gelfand, J. Dant, E. S. Brooks, D. E. Krantz, A. DiAntonio, Increased expression of the Drosophila vesicular glutamate transporter leads to excess glutamate release and a compensatory decrease in quantal content. *J. Neurosci.* **24**, 10466–10474 (2004).
12. D. K. Dickman, J. A. Horne, I. A. Meinertzhagen, T. L. Schwarz, A slowed classical pathway rather than kiss-and-run mediates endocytosis at synapses lacking synaptojanin and endophilin. *Cell* **123**, 521–533 (2005).
13. C. K. Chen, C. Bregere, J. Paluch, J. F. Lu, D. K. Dickman, K. T. Chang, Activity-dependent facilitation of Synaptojanin and synaptic vesicle recycling by the Minibrain kinase. *Nat. Commun.* **5**, 4246 (2014).
14. P. Goel, D. Dufour Bergeron, M. A. Bohme, L. Nunnelly, M. Lehmann, C. Buser, A. M. Walter, S. J. Sigrist, D. Dickman, Homeostatic scaling of active zone scaffolds maintains global synaptic strength. *J. Cell Biol.* **218**, 1706–1724 (2019).
15. M. A. Gavino, K. J. Ford, S. Archila, G. W. Davis, Homeostatic synaptic depression is achieved through a regulated decrease in presynaptic calcium channel abundance. *eLife* **4**, e05473 (2015).
16. X. Li, P. Goel, J. Wondolowski, J. Paluch, D. Dickman, A glutamate homeostat controls the presynaptic inhibition of neurotransmitter release. *Cell Rep.* **23**, 1716–1727 (2018).
17. S. J. Gratz, P. Goel, J. J. Bruckner, R. X. Hernandez, K. Khateeb, G. T. Macleod, D. Dickman, K. M. O'Connor-Giles, Endogenous tagging reveals differential regulation of Ca^{2+} channels at single active zones during presynaptic homeostatic potentiation and depression. *J. Neurosci.* **39**, 2416–2429 (2019).
18. A. DiAntonio, S. A. Petersen, M. Heckmann, C. S. Goodman, Glutamate receptor expression regulates quantal size and quantal content at the Drosophila neuromuscular junction. *J. Neurosci.* **19**, 3023–3032 (1999).
19. P. S. Pinheiro, C. Mulle, Presynaptic glutamate receptors: Physiological functions and mechanisms of action. *Nat. Rev. Neurosci.* **9**, 423–436 (2008).
20. M. Scanziani, P. A. Salin, K. E. Vogt, R. C. Malenka, R. A. Nicoll, Use-dependent increases in glutamate concentration activate presynaptic metabotropic glutamate receptors. *Nature* **385**, 630–634 (1997).
21. T. Takahashi, I. D. Forsythe, T. Tsujimoto, M. Barnes-Davies, K. Onodera, Presynaptic calcium current modulation by a metabotropic glutamate receptor. *Science* **274**, 594–597 (1996).
22. J. N. Kew, J. M. Ducarre, M. C. Pflimlin, V. Mutel, J. A. Kemp, Activity-dependent presynaptic autoinhibition by group II metabotropic glutamate receptors at the perforant path inputs to the dentate gyrus and CA1. *Neuropharmacology* **40**, 20–27 (2001).
23. L. Bogdanik, R. Mohrmann, A. Ramaekers, J. Bockaert, Y. Grau, K. Broadie, M. L. Parmentier, The Drosophila metabotropic glutamate receptor DmGluRA regulates activity-dependent synaptic facilitation and fine synaptic morphology. *J. Neurosci.* **24**, 9105–9116 (2004).
24. H. Takago, Y. Nakamura, T. Takahashi, G protein-dependent presynaptic inhibition mediated by AMPA receptors at the calyx of Held. *Proc. Natl. Acad. Sci. U.S.A.* **102**, 7368–7373 (2005).
25. J. Lerma, J. M. Marques, Kainate receptors in health and disease. *Neuron* **80**, 292–311 (2013).
26. Z. Padamsey, R. Tong, N. Emptage, Glutamate is required for depression but not potentiation of long-term presynaptic function. *eLife* **6**, e29688 (2017).
27. J. Dudel, S. W. Kuffler, Presynaptic inhibition at the crayfish neuromuscular junction. *J. Physiol.* **155**, 543–562 (1961).
28. P. Rudomin, R. F. Schmidt, Presynaptic inhibition in the vertebrate spinal cord revisited. *Exp. Brain Res.* **129**, 1–37 (1999).
29. S. Takayanagi-Kiya, K. Zhou, Y. Jin, Release-dependent feedback inhibition by a presynaptically localized ligand-gated anion channel. *eLife* **5**, (2016).
30. L. G. Wu, P. Saggau, Presynaptic inhibition of elicited neurotransmitter release. *Trends Neurosci.* **20**, 204–212 (1997).
31. R. Benton, K. S. Vannice, C. Gomez-Diaz, L. B. Vosshall, Variant ionotropic glutamate receptors as chemosensory receptors in Drosophila. *Cell* **136**, 149–162 (2009).
32. H. Kamiya, Kainate receptor-dependent presynaptic modulation and plasticity. *Neurosci. Res.* **42**, 1–6 (2002).
33. C. M. Schuster, Glutamatergic synapses of Drosophila neuromuscular junctions: A high-resolution model for the analysis of experience-dependent potentiation. *Cell Tissue Res.* **326**, 287–299 (2006).
34. S. Nagarkar-Jaiswal, P. T. Lee, M. E. Campbell, K. Chen, S. Anguiano-Zarate, M. C. Gutierrez, T. Busby, W. W. Lin, Y. He, K. L. Schulze, B. W. Booth, M. Evans-Holm, K. J. Venken, R. W. Levis, A. C. Spradling, R. A. Hoskins, H. J. Bellen, A library of MiMICs allows tagging of genes and reversible, spatial and temporal knockdown of proteins in Drosophila. *eLife* **4**, e05338 (2015).
35. A. J. Wolstenholme, Glutamate-gated chloride channels. *J. Biol. Chem.* **287**, 40232–40238 (2012).
36. R. E. Hibbs, E. Gouaux, Principles of activation and permeation in an anion-selective Cys-loop receptor. *Nature* **474**, 54–60 (2011).
37. D. F. Cully, P. S. Paress, K. K. Liu, J. M. Schaeffer, J. P. Arena, Identification of a Drosophila melanogaster glutamate-gated chloride channel sensitive to the antiparasitic agent avermectin. *J. Biol. Chem.* **271**, 20187–20191 (1996).
38. S. Molina-Obando, J. F. Vargas-Fique, M. Henning, B. Gur, T. M. Schladt, J. Akhtar, T. K. Berger, M. Silies, ON selectivity in the Drosophila visual system is a multisynaptic process involving both glutamatergic and GABAergic inhibition. *eLife* **8**, e49373 (2019).

39. S. Fendl, R. M. Vieira, A. Borst, Conditional protein tagging methods reveal highly specific subcellular distribution of ion channels in motion-sensing neurons. *eLife* **9**, e62953 (2020).
40. S. Kondo, T. Takahashi, N. Yamagata, Y. Imanishi, H. Katow, S. Hiramatsu, K. Lynn, A. Abe, A. Kumaraswamy, H. Tanimoto, Neurochemical organization of the drosophila brain visualized by endogenously tagged neurotransmitter receptors. *Cell Rep.* **30**, 284–297.e5 (2020).
41. S. Viswanathan, M. E. Williams, E. B. Bloss, T. J. Stasevich, C. M. Speer, A. Nern, B. D. Pfeiffer, B. M. Hooks, W. P. Li, B. P. English, T. Tian, G. L. Henry, J. J. Macklin, R. Patel, C. R. Gerfen, X. Zhuang, Y. Wang, G. M. Rubin, L. L. Looger, High-performance probes for light and electron microscopy. *Nat. Methods* **12**, 568–576 (2015).
42. J. Rohrbough, K. Broadie, Electrophysiological analysis of synaptic transmission in central neurons of Drosophila larvae. *J. Neurophysiol.* **88**, 847–860 (2002).
43. R. W. Daniels, C. A. Collins, K. Chen, M. V. Gelfand, D. E. Featherstone, A. DiAntonio, A single vesicular glutamate transporter is sufficient to fill a synaptic vesicle. *Neuron* **49**, 11–16 (2006).
44. K. E. Poskanzer, K. W. Marek, S. T. Sweeney, G. W. Davis, Synaptotagmin I is necessary for compensatory synaptic vesicle endocytosis in vivo. *Nature* **426**, 559–563 (2003).
45. J. Bai, Z. Hu, J. S. Dittman, E. C. Pym, J. M. Kaplan, Endophilin functions as a membrane-bending molecule and is delivered to endocytic zones by exocytosis. *Cell* **143**, 430–441 (2010).
46. C. K. Yao, Y. Q. Lin, C. V. Ly, T. Ohyama, C. M. Haueter, V. Y. Moiseenkova-Bell, T. G. Wensel, H. J. Bellen, A synaptic vesicle-associated Ca^{2+} channel promotes endocytosis and couples exocytosis to endocytosis. *Cell* **138**, 947–960 (2009).
47. S. Perry, P. Goel, N. L. Tran, C. Pinales, C. Buser, D. L. Miller, B. Ganetzky, D. Dickman, Developmental arrest of *Drosophila* larvae elicits presynaptic depression and enables prolonged studies of neurodegeneration. *Development* **147**, dev186312 (2020).
48. P. Goel, M. Khan, S. Howard, G. Kim, B. Kiragasi, K. Kikuma, D. Dickman, A screen for synaptic growth mutants reveals mechanisms that stabilize synaptic strength. *J. Neurosci.* **39**, 4051–4065 (2019).
49. S. M. Wojcik, J. S. Rhee, E. Herzog, A. Sigler, R. Jahn, S. Takamori, N. Brose, C. Rosenmund, An essential role for vesicular glutamate transporter 1 (VGLUT1) in postnatal development and control of quantal size. *Proc. Natl. Acad. Sci. U.S.A.* **101**, 7158–7163 (2004).
50. R. Chang, J. Eriksen, R. H. Edwards, The dual role of chloride in synaptic vesicle glutamate transport. *eLife* **7**, (2018).
51. J. S. Dittman, T. A. Ryan, The control of release probability at nerve terminals. *Nat. Rev. Neurosci.* **20**, 177–186 (2019).
52. F. Felmy, E. Neher, R. Schneggenburger, The timing of phasic transmitter release is Ca2+–dependent and lacks a direct influence of presynaptic membrane potential. *Proc. Natl. Acad. Sci. U.S.A.* **100**, 15200–15205 (2003).
53. B. Kiragasi, J. Wondolowski, Y. Li, D. K. Dickman, A presynaptic glutamate receptor subunit confers robustness to neurotransmission and homeostatic potentiation. *Cell Rep.* **19**, 2694–2706 (2017).
54. G. Ashrafi, Z. Wu, R. J. Farrell, T. A. Ryan, GLUT4 mobilization supports energetic demands of active synapses. *Neuron* **93**, 606–615.e3 (2017).
55. R. W. Daniels, B. R. Miller, A. DiAntonio, Increased vesicular glutamate transporter expression causes excitotoxic neurodegeneration. *Neurobiol. Dis.* **41**, 415–420 (2011).
56. S. Mahmoud, M. Gharagozloo, C. Simard, D. Gris, Astrocytes maintain glutamate homeostasis in the CNS by controlling the balance between glutamate uptake and release. *Cell* **8**, 184 (2019).
57. T. Rival, L. Soustelle, C. Strambi, M. T. Besson, M. Iche, S. Birman, Decreasing glutamate buffering capacity triggers oxidative stress and neuropil degeneration in the Drosophila brain. *Curr. Biol.* **14**, 599–605 (2004).
58. S. Lee, Y. Zhang, M. Chen, Z. J. Zhou, Segregated glycine-glutamate co-transmission from vGluT3 amacrine cells to contrast-suppressed and contrast-enhanced retinal circuits. *Neuron* **90**, 27–34 (2016).
59. T. V. Waseem, S. V. Fedorovich, Presynaptic glycine receptors influence plasma membrane potential and glutamate release. *Neurochem. Res.* **35**, 1188–1195 (2010).
60. S. Lewis, Synaptic transmission: A closer look at presynaptic GABA(B) receptors. *Nat. Rev. Neurosci.* **11**, 664 (2010).
61. S. Kim, M. L. Wallace, M. El-Rifai, A. R. Knudsen, B. L. Sabatini, Biophysical demonstration of co-packaging of glutamate and GABA in individual synaptic vesicles in the central nervous system. *bioRxiv*, 2021.2003.2023.436594 , (2021).
62. R. Cohn, I. Morantte, V. Ruta, Coordinated and compartmentalized neuromodulation shapes sensory processing in drosophila. *Cell* **163**, 1742–1755 (2015).
63. S. J. Gratz, F. P. Ukken, C. D. Rubinstein, G. Thiede, L. K. Donohue, A. M. Cummings, K. M. O'Connor-Giles, Highly specific and efficient CRISPR/Cas9-catalyzed homology-directed repair in Drosophila. *Genetics* **196**, 961–971 (2014).
64. K. Kikuma, X. Li, S. Perry, Q. Li, P. Goel, C. Chen, D. Kim, N. Stavropoulos, D. Dickman, Cul3 and insomniac are required for rapid ubiquitination of postsynaptic targets and retrograde homeostatic signaling. *Nat. Commun.* **10**, 2998 (2019).
65. A. R. Poe, B. Wang, M. L. Sapar, H. Ji, K. Li, T. Onabajo, R. Fazliyeva, M. Gibbs, Y. Qiu, Y. Hu, C. Han, Robust CRISPR/Cas9-mediated tissue-specific mutagenesis reveals gene redundancy and perdurance in drosophila. *Genetics* **211**, 459–472 (2019).
66. X. Chen, W. Ma, S. Zhang, J. Paluch, W. Guo, D. K. Dickman, The BLOC-1 subunit pallidin facilitates activity-dependent synaptic vesicle recycling. *eNeuro* **4**, ENEURO.0335–ENEU16.2017 (2017).
67. J. M. Mackler, J. A. Drummond, C. A. Loewen, I. M. Robinson, N. E. Reist, The C(2)B Ca(2+)-binding motif of synaptotagmin is required for synaptic transmission in vivo. *Nature* **418**, 340–344 (2002).
68. X. Li, P. Goel, C. Chen, V. Angajala, X. Chen, D. K. Dickman, Synapse-specific and compartmentalized expression of presynaptic homeostatic potentiation. *eLife* **7**, e34338 (2018).
69. P. Goel, X. Li, D. Dickman, Estimation of the readily releasable synaptic vesicle pool at the drosophila larval neuromuscular junction. *Bio Protoc.* **9**, e3127 (2019).

Acknowledgments: We thank D. Krantz (UCLA, Los Angeles, CA, USA), M. Heckmann (Würzburg, Germany), M. Müller (Zürich, Switzerland), and R. Edwards (UCSF, San Francisco, CA, USA) for important discussions on GluClα and vGlut and G. Macleod and R. Hernandez (Florida Atlantic University, Jupiter, FL, USA) for advice on Ca^{2+} imaging and analysis. We also thank M. Silies (Johannes Gutenberg-Universität Mainz, Mainz, Germany), S. Fendl and A Borst (Max Planck Institute of Neurobiology, Martinsried, Germany), V. Ruta (Rockefeller Institute, New York, USA), and M.-L. Parmentier (Institut de Génomique Fonctionnelle, Montpellier, France) for sharing reagents. We acknowledge N. Tran for assistance with *Drosophila* strains and the Bloomington *Drosophila* Stock Center and the Developmental Studies Hybridoma Bank for additional stocks and reagents (NIH grant P40OD018537). **Funding:** This study was supported by grants from the National Institute of Neurological Disease and Stroke to D.D. (NS111414). **Author contributions:** X.L. and D.D. conceived and designed the study. C.C. and Y.H. performed some imaging and electrophysiological experiments. Z.S. performed the GPCR candidate screen, and X.C. generated the *GluClα* transgenes. All other experiments were performed by X.L. The manuscript was written by X.L. and D.D. with feedback from the other authors. **Competing interests:** The authors declare that they have no competing interests. **Data and materials availability:** All data needed to evaluate the conclusions in the paper are present in the paper and/or the Supplementary Materials. Further information and requests for reagents should be directed to and will be fulfilled by the lead contact D.D. (dickman@usc.edu).

Submitted 22 April 2021
Accepted 14 October 2021
Published 1 December 2021
10.1126/sciadv.abj1215